

1 Classification of tall tower meteorological variables and
2 forecasting wind speeds in Columbia, Missouri

3 Sarah Balkissoon^{1, 2}, Neil Fox¹, Anthony Lupo¹, Sue Ellen Haupt³, and Stephen
4 G. Penny^{4,2}

5 ¹Atmospheric Science Program, School of Natural Resources, University of
6 Missouri, USA

7 ² Cooperative Institute for Research in Environmental Sciences, Boulder, Colorado,
8 USA

9 ³Research Applications Lab, National Center for Atmospheric Research, Boulder,
10 Colorado, USA

11 ⁴Sofar Ocean, San Francisco, California, USA

12 June 20, 2023

13 **Abstract**

14 The wind speeds given in 10-minute intervals is forecast using multiple methods inclusive of
15 persistence, statistical methods of ARIMA as well as artificial intelligence methods of Artificial
16 Neural Networks. Tall tower meteorological variables in Columbia, Missouri are clustered
17 using Self-Organizing Maps after the optimal number of clusters was determined using the
18 Elbow and Silhouette methods among others. The optimal number of clusters, k was given
19 as 4 for all methods. The data were then grouped into three Intervals which consisted of
20 approximately 50 percent and over of vectors or rows from the data frame. These intervals
21 were then used as training and testing for the forecast models of Long Short-Term Memory
22 Networks with pressure and wind speeds as inputs as well as lagged wind speeds as inputs.
23 Other models using these intervals in our analyses include Moving Autoregressive Integrated
24 Moving Average (ARIMA) and persistence. From the results obtained from the ARIMA, the
25 metric of the root mean square error (RMSE) ranged from approximately 0.6 to 1.0 m s^{-1} for
26 forecast horizon 2 to 12 in increments of 2. Interval2 had the upper and lower values and thus
27 showed most variability in errors because it encompassed most of spring, all of summer and the
28 beginning of fall. The moving ARIMA showed lower errors than the LSTM with pressure and
29 wind speeds inputs for all the intervals. This may be attributed to the difficulty in representing
30 the system's non-linearity and high dimensionality by using just the wind speeds and pressure
31 as inputs. The lagged co-ordinates of the wind speed was then examined and used as inputs for
32 the LSTM. The metric used for the evaluation of prediction of the forecast horizons of 60, 120,
33 180, 240, 300 and 360 minutes or 1, 2, 3, 4, 5 and 6 hours ahead is the Normalized Root Mean
34 Square Error (NRMSE). These models were compared to the benchmark model of persistence.
35 It was determined that all of the models beat persistence and the LSTM with the lag series
36 outperforms the LSTM with pressure and wind speed as inputs. The Moving ARIMA is now
37 beaten by the lagged series LSTM in all intervals for at least 2 time forecast horizons of 60
38 and 120 minutes or 1 and 2 hours. It is thus shown that the Artificial Neural Network method
39 with the lagged series inputs is the best performing model.

40 **Keywords:** Self-Organizing Maps (SOMs), Autoregressive Integrated Moving Average
41 (ARIMA), Long Short-Term Memory (LSTM) Networks

43 **1 Introduction**

44 **1.1 Wind speeds**

45 Wind speeds closer to the ground are subjected to resistance and friction. Even though these
46 winds are highly positively correlated with each other, the correlations grow weaker with height as
47 noted in both this study and Cao et al.'s [9]. Due to local surface characteristics and large scale
48 forcing mechanisms such as pressure and temperature differences, wind is one of the most difficult
49 meteorological variables to forecast [28]. Also, since the atmosphere is highly nonlinear and high
50 dimensional, it is especially difficult to forecast this variable in the much needed higher resolutions
51 and longer time horizons [15]. The higher resolution shows more details of the faster variations in
52 wind speeds caused by turbulence and other factors. The importance of such forecasts stems from
53 the ability to aid in the scheduling, dispatching and adjusting electricity reservations [15]. In our
54 work we are looking at short term forecasting at high resolution (10 minute wind speeds at hub
55 height).

56 **1.2 Forecasting of wind speeds**

57 Due to the stochastic nature of wind speeds, forecasting this variable is important for its optimal
58 integration into the power grids [27]. These short term forecasts, can be used by plant managers to
59 adjust turbine components to achieve more efficiency. Another advantage of short term forecasts
60 is the ability to make turbines operable closer to extreme weather events before shutting down.
61 Daily short term forecasts are also important as they relate to the operability of the turbines in
62 terms of their cut-in and cut-off wind speeds as they aid in the reduction of structural damage to
63 infrastructure [9].

64 There are numerous methods that have been used to forecast wind speed values, some of which
65 are illustrated in Figure 3. Please see the acronyms ¹ associated with this chart. The methods
66 incorporated in this paper are Artificial Intelligence (AI) methods which are compared to statisti-
67 cal models as well as the benchmark of persistence. The significant difference between these two
68 methods is that statistical multiple linear regression is written in terms of a set of linear operators
69 whilst Artificial Neural Networks(ANNs) are representative of a linear combination of simple non-
70 linear functions [4]. A mapping is done from random input vectors to output vectors without the
71 assumption that there is a fixed relationship between the two [19]. ANNs have the ability to learn
72 from past data by recognizing patterns among the observations and using these to forecast into the
73 future [19]. Research has indicated the superiority in prediction accuracy of ANNs to statistical
74 regression especially as the non-linearity of the problem increases [4]. Previous studies, namely [2]
75 and [3], done in Missouri, found the wind speeds to be chaotic in nature, hence motivating the
76 choice of this method to address the complexity and non-linearity of the data.

77 **1.3 Wind Power**

78 From the relationship $P = \frac{1}{2}\rho AV^3$ where P is the available power at the turbine, ρ is the density of
79 air, A is the area swept by the turbine and V is the wind speed, the two meteorological variables
80 which determines the available turbine power are ρ and V . The latter variable has the greater
81 influence as the power varies as the cube of V . The air density is dependent on pressure and
82 temperature as seen from the following equation [21]

$$\rho = D \left(\frac{273.15}{T} \right) \left[\frac{B - 0.3783e}{760} \right] \quad (1)$$

83 where D is 1.168 kg/m^3 - the density of dry air at standard atmospheric temperature (25°C) and
84 pressure (100 kPa) and B is the barometric pressure in torr, e is the moist air vapour pressure in
85 torr. Hence, as seen in subsequent sections of the methods, these two meteorological parameters,
86 will be considered, together with wind speeds, when determining the inputs to the Neural Network.

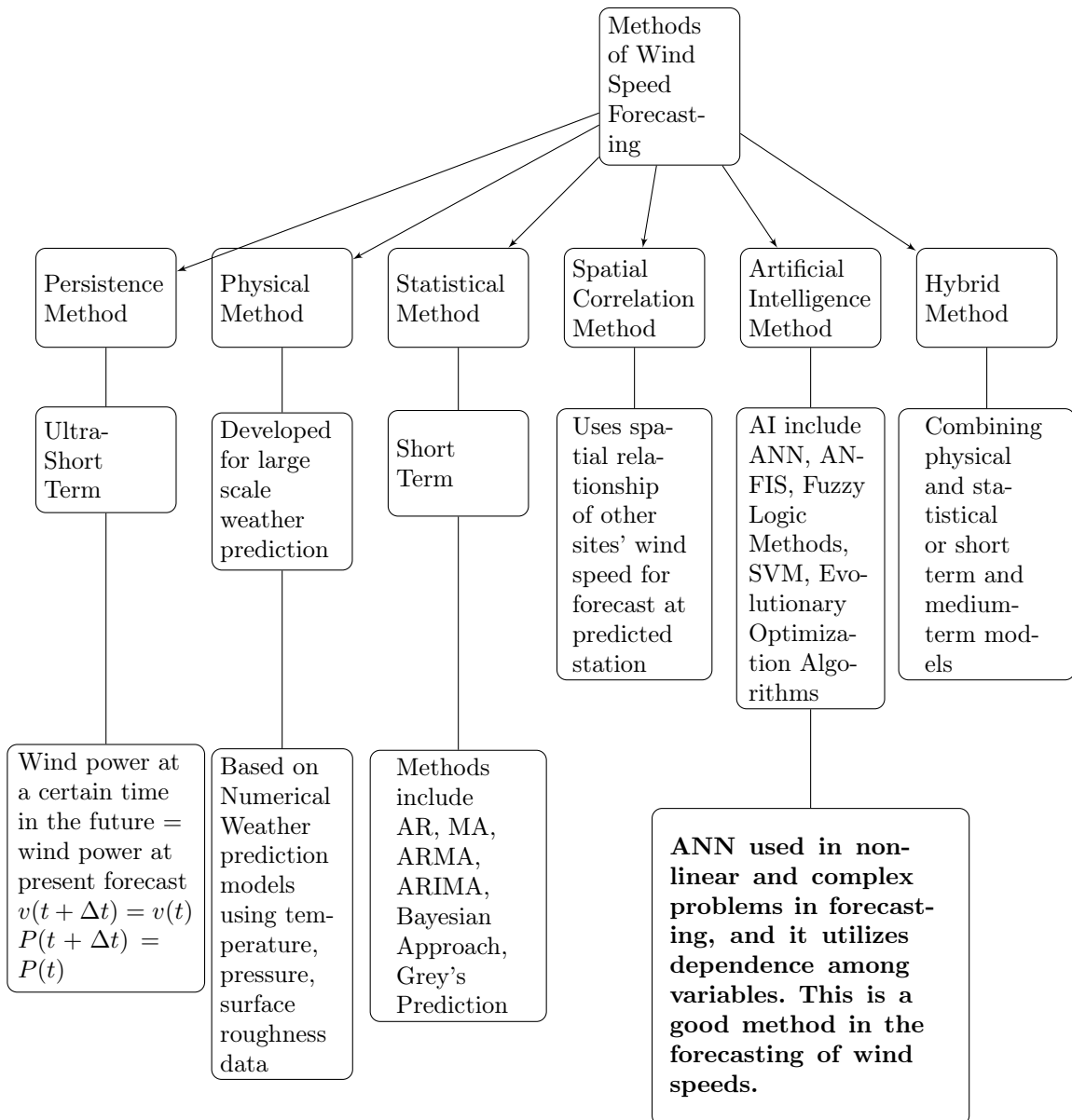
¹ AI-Artificial Intelligence, ANN-Artificial Neural Networks, ANFIS-Adaptive Neuro-Fuzzy Interface System, SVM-Support Vector Machine, AR-Auto-Regressive, MA-Moving Average, ARMA-Auto-Regressive Moving Average, ARIMA-Auto-Regressive Integrated Moving Average

87 1.4 Literature Review

88 From [10], comparative analysis of ARIMA and LSTM models in predicting hourly wind speeds
89 indicated the RMSE to be less than of the ARIMA method. An analysis of the existing literature
90 and the studies done by [10] showed that for smaller datasets, ARIMA performed better whilst for
91 larger datasets, deep learning techniques such as LSTM outperforms the statistical methods such
92 as ARIMA. Another study done by [33] forecasts 10-minute wind speeds as done in our study, but
93 uses fuzzy set theory to conduct attribute reduction of the factors affecting the wind speeds instead
94 of the magnitude correlation plot. This determined what were the inputs into the LSTM model.
95 This simplified input improves upon the accuracy as well as the speed of the model [33]. In [14],
96 dimensionality reduction of the meteorological data that affects the wind speed is also conducted.
97 They instead utilizes principal component analysis (PCA). It was found that this case had the
98 most improvements in terms of errors when compared to models' inputs of the historical wind
99 speed data and the other exogenous variables. In reference [13], the authors compared the results
100 of two models, LSTM and Support-Vector Machine (SVM) in the prediction of wind speeds. It was
101 determined that of the two algorithms the LSTM incurred the lower RMSE than that of the SVM
102 due to the LSTM's ability to remember patterns for a longer duration. [1] showed the superiority
103 in model performance of hybrid simulations. This study, using the metric of RMSE, determined
104 that the LSTM-ARIMA model had less forecasting errors when compared to the LSTM and SVM
105 models. Another paper that incorporates clustering to select the training samples before feeding
106 them to the LSTM is [31]. However, this is done for day-ahead forecasting. They utilized a density
107 based spatial clustering (DBSCAN), deep feature extraction and LSTM forecasting in their study.
108 Their proposed model out performed the benchmark methods of random forest (RF), least square
109 support vector regression (LSSVR) and back propagation neural network (BPNN), by at least 17%
110 [31]. In another comparative study of forecasting hourly wind speeds for a year, Neural Networks
111 was compared with the statistical method of ARMA in which the ARMA was outperformed by
112 all the other methods; the feed forward neural network (FNN), recurrent neural network (RNN),
113 LSTM and the gated recurrent unit (GRU)[34]. The ANN which are utilized for the purpose of
114 short term forecasting of wind speeds usually perform better than the time series methods with a
115 few exceptions [34]. The authors considered the variables that were also investigated in this study
116 in the prediction of the target variable; these are wind direction, wind speed with one time step
117 lag, pressure and temperature. After various permutations of the inputs, it was found that the
118 wind speed with the one time lag had the largest correlation with the wind speed and as such it
119 was deemed the most important feature [34]. In [12], the variations of inputs into a LSTM as well
120 as a 1D-CNN were also investigated.

121 The objective of this paper is to apply multiple forecasting techniques of tall tower data in
122 Missouri; persistence as a benchmark, statistical methods of ARIMA and ANN techniques in clus-
123 tering and subsequently forecasting using LSTM. The novelty of this work includes the usage of
124 the competitive learning Neural Network, SOMs, in the clustering of the data with similar patterns
125 which are then the inputs into the LSTM. This feature of data mining, clustering of data, allow for
126 the preprocessing of the data and thus the accurate development of forecasting models [13] [31].
127 The forecasting of tall tower data in Columbia, MO for this scale is carried out; short term forecasts
128 at high resolution is conducted. The proposed methodology is tested using real -world tall tower
129 data and it outperforms other known prediction methods. The subsequent structure of the paper
130 is as follows. Section 2 gives the data used in this study, section 3 introduces the concepts of the
131 methods incorporated in this paper, section 4 discusses the results whilst sections 5 gives the future
132 analyses that can be conducted and the conclusion of the paper collectively.

Figure 1: Methods for wind speed forecasting



133 2 Data

134 Columbia, Missouri is located in $038^{\circ}53.270'N$ latitude and $092^{\circ}15.820'W$ longitude and has a
135 site elevation of 255m as seen in Figure 2. Ten-minute tall tower wind speed, wind direction
136 and temperature data in 2009 from this region were used in our study [11]. The respective units
137 are $m s^{-1}$, degrees and degrees Celsius, respectively. The anemometer orientations were 120° and
138 300° for the tall tower height of 68 m. Channels 1 and 2 represent the respective wind speed times
139 series. The larger of the wind speed values at each time step were taken and labelled as Max1. The
140 wind direction time series at this height level was given from channel 7 and sine of these angles was
141 labelled as Direction1. The temperature time series from 2 m logger height were also utilized in
142 our analyses, taken from channel 11, it is referred to as Temp. Hourly maximum pressure data was
143 taken from University of Missouri, Extension's Missouri Historical Agricultural Weather Database.
144 Each hourly pressure value was repeated five times. This time series, labelled as Pressure, along
145 with Max1, Direction1 and Temp were combined and used in all of the analyses for Columbia68 as
146 detailed in the Methods section below.

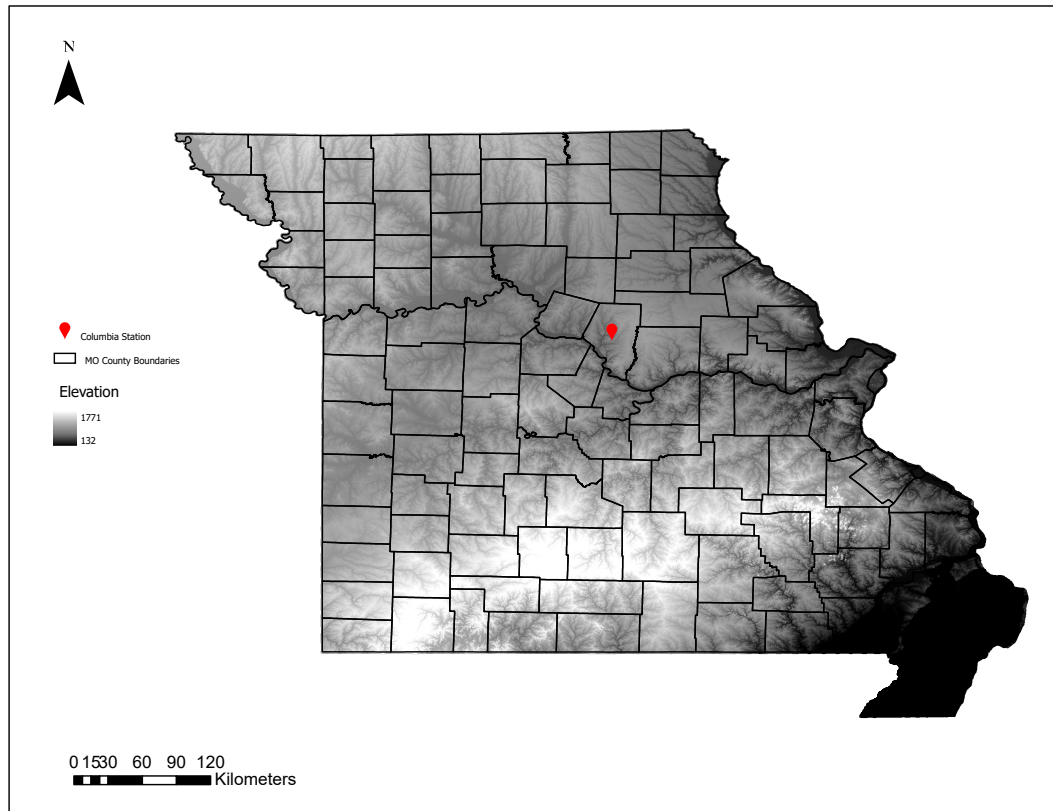


Figure 2: Tall tower location

147 3 Methods

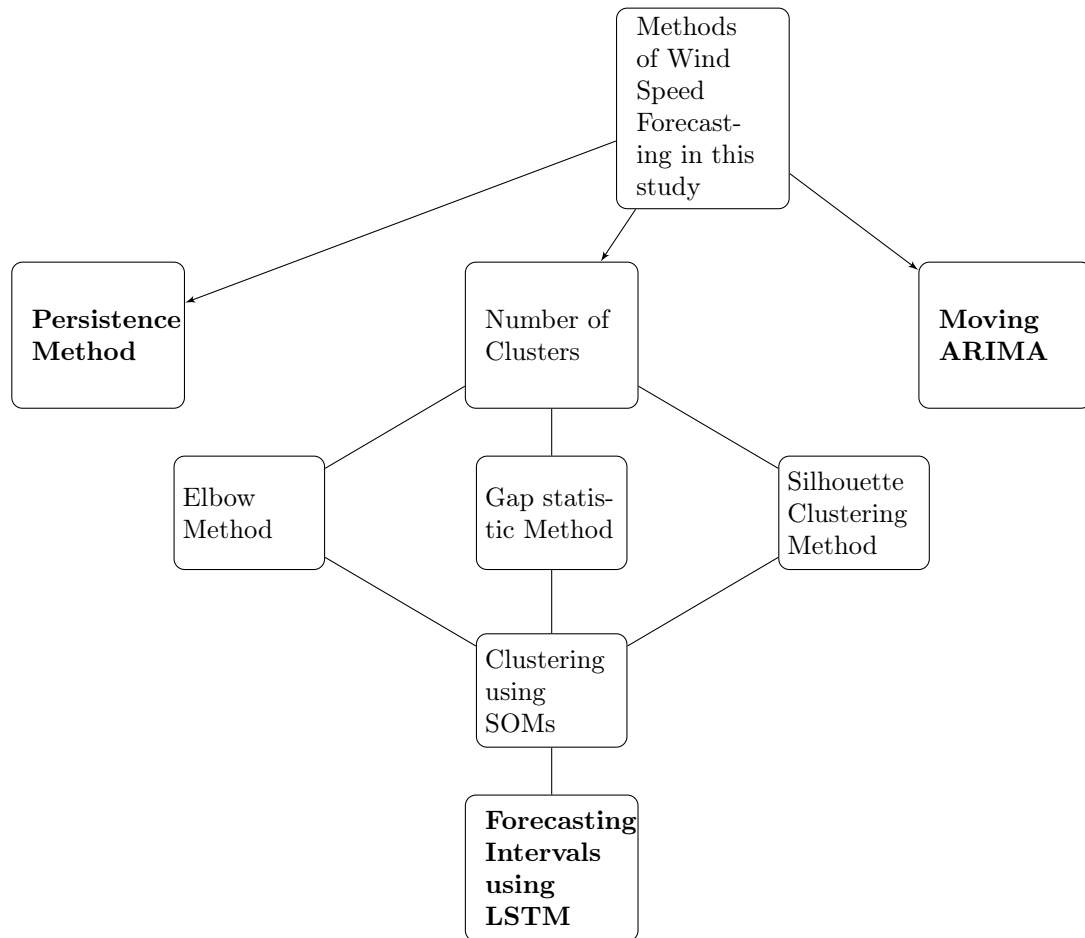
148 Artificial Neural Networks (ANN) have to date been applied to a multitude of fields in solving com-
149 plex problems. These data-driven models are utilized especially as physically-based mathematical
150 models are difficult to construct given the high non-linearity of natural systems [20]. As defined
151 by Basheer and Hajmeer [4] and Ramasamy et al. [25] , ANNs can be considered as a system of
152 densely interconnected processing elements, also called artificial neurons or nodes, which have the
153 ability to conduct parallel computations of input data .Complex relationships are derived from the

154 input and the output. The input variables are multiplied by weights and biases are added to these
155 products. These are then passed through transfer functions for the generation of the outputs [25].

156 ANNs, being abstractions of biological systems, have the advantages of processing data that are
157 highly nonlinear. These robust systems have the ability to learn and generalize imprecise and fuzzy
158 data [4]. Data are allowed to be processed faster and have a better fit amidst inaccuracies from
159 measurement errors. The system in its learning is self updating and has the ability to unlearn data
160 as well [4].

161 There are many applications of ANNs, which include modelling, classification, pattern recogni-
162 tion and multivariate data analysis problems [4] [25]. Here, we will focus our attention on the
163 clustering of the data into various clusters and then on subsequent modelling and forecasting. Clus-
164 tering as described by [4], is formed by investigating the similarities and differences of the inputs
165 based on their inter-correlations. Kohonen networks or Self-Organizing Feature Maps (SOMs), the
166 unsupervised learning ANN where the actual values are not required for the training set, are used
167 in this study. Forecasting is also done by training the ANN using a training set of historical data. A
168 Recurrent Neural Network (RNN) is utilized especially for its dynamic memory capabilities where
169 the outputs of neurons are fed as inputs to the same neurons or other neurons in the preceding
170 layers [4]. A general overview of the methods incorporated in this study is depicted in the flow
171 diagram below. More details of these methods are given in the following sub-sections.

Figure 3: Methods for wind speed forecasting utilized in this study



172 3.1 Methods determining the number of clusters

173 Clustering analyses as mentioned in [22], are statistical methods which are used to partition multi-
174 variate data into subsets. There are numerous methods that can be used to determine the optimal

175 number of clusters to classify the data into relatively homogeneous groups, such as the Elbow
 176 Method, Silhouette Analysis and Gap Statistic. These methods, which are used in this study,
 177 are outlined below. We have considered in the analyses this multivariate data set (of length n)
 178 of variables wind speed, direction, temperature and pressure. We denote these points as x_i for
 179 $i = 1, \dots, n$.

180 The Elbow Method is determined by plotting the within-cluster sum of squares (WCSS) against
 181 the number of clusters, say k . The $WCSS(k)$ gives the sum of the squared distances between
 182 each data point, say x_i , in all clusters and their associated centroids denoted as \bar{x}_j (which is the
 183 geometric center or the arithmetic mean position of all the points in the plane figure). This can be
 184 written as follows.

$$WCSS(k) = \sum_{j=1}^k \sum_{x_i \in \text{cluster}_j} \|x_i - \bar{x}_j\|^2 \quad (2)$$

185 The changes in $WCSS$ with a range of k determines the optimal number of clusters in accordance
 186 with the Elbow method. The value in which k elbows or the point where the rate of decrease in
 187 $WCSS$ is relatively minimal when compared to its previous k values.

188 The Silhouette Clustering method was also used in our analysis. This method examines the
 189 within cluster-consistency by comparing how similar objects from a cluster are to another. Its
 190 value, $S(i)$ range from -1 to 1 where the lower end of the interval indicates that the configuration
 191 has too much or few clusters. The closer this value is to 1 however, is indicative of an object that
 192 is well matched to its cluster or poorly matched to the other clusters.

193 The mean similarity of point i and all other points in the same cluster, C_i , is given by equation 3
 194 where $|C_i|$ denotes the number of elements in C_i and $d(i, j)$ give the distances between data points i
 195 and j in cluster C_i . In this average the distances, $d(i, i)$ are not considered hence the consideration
 196 of $|C_i| - 1$ in the formulation below.

$$a_i = \frac{1}{|C_i| - 1} \sum_{j \in C_i, i \neq j} d(i, j) \quad (3)$$

197 The smallest mean dissimilarity of point i and all the other points of another cluster, C_k , is
 198 given by b_i in equation 4.

$$b_i = \min_{k \neq i} \frac{1}{|C_k|} \sum_{j \in C_k} d(i, j) \quad (4)$$

199 This is the second best fit cluster for point i based on the distance metric. The Silhouette value
 200 for point i , we define as S_i , is given in terms of a_i and b_i as seen in equation 5.

$$S_i = \begin{cases} \frac{(b_i) - (a_i)}{\max\{a_i, b_i\}} & \text{if } |C_i| > 1 \\ 0 & \text{if } |C_i| = 1 \end{cases} \quad (5)$$

201 This can be further simplified as seen below, depending on the inequality relations between the
 202 mean similarity and dissimilarity.

$$S_i = \begin{cases} 1 - \frac{a_i}{b_i} & \text{if } a_i < b_i \\ 0 & \text{if } a_i = b_i \\ \frac{b_i}{a_i} - 1 & \text{if } a_i > b_i \end{cases} \quad (6)$$

203 The Gap Statistic, another consideration used in this paper, is outlined as follows. As previously
 204 denoted, let C_i be the i^{th} Cluster and $|C_i|$ be representative of the number of elements in this cluster.
 205 Let the pairwise distances between elements say i and j in C_i , d_i , be given by equation 7.

$$d_i = \sum_{i, j \in C_i} d(i, j) \quad (7)$$

206 For a given number of clusters k , the within cluster distance for that particular partitioning P_k ,
 207 is given by equation 8. A better classification is indicative of a smaller W_k value.

$$W_k = \sum_{i=1}^k \frac{1}{2|C_i|} d_i \quad (8)$$

Considering the data in which the 'true' number of clusters is given by G , W_k should drop as k increases until it reaches G where it will decrease at a much slower rate. Thus, there will be an 'elbow' point in W_k ; this k value corresponds to the optimal number of clusters. The Gap Method is used to compare the original data with the expected curve, $E_n^* \{\log(W_k)\}$ where E_n^* gives the expectation of sample n from the reference distribution. The Gap Statistic is the value of k which maximizes $Gap_n(k)$ or from equation 9, the cluster value where W_k is at the furthest distance from the expected curve [32].

$$Gap_n(k) = E_n^* \{\log(W_k)\} - \log(W_k) \quad (9)$$

3.2 Self Organizing Maps (SOM)

A Self Organizing Map (SOM) is an unsupervised clustering method as there is no additional information being supplied to the model by a 'supervisor' [16]. In this model, high-dimensional data sets are reduced to the two-dimensional map in which nodes with most similarity are nearest to each other and vice-versa [23]. It does this dimensionality reduction via the usage of cluster centers which can then be interpreted as an 'abstract representation' of any given vector from that particular cluster [16]. It preserves topology where vectors that are near in input space are also mapped to nearby neurons in the SOM [22][23]. This resulting map is a projection of a multidimensional space rather than a geographical space [23]. There are two modes of operation, training which builds the map using input examples through a method called vector quantization and mapping which classifies new input vectors [7].

This Kohonen Neural Network is used in many applications [30] such as Pearce et al.'s air quality classifications [23] and in geoscience for the extraction of climate and atmospheric circulation patterns [16]. Previous studies using SOMs also include Berkovic's [5] determination of the wind regimes, choosing from various map sizes, the number of nodes in the rows and columns. However in our study, since we utilized SOMs for the purposes for clustering our data to be later incorporated in our forecasting algorithm, we defined our map size based on the formulation written in [29]. The number of neurons, M of the map is determined from the number of observations, N . It is given by the following expression [7].

$$M \approx 5\sqrt{N} \quad (10)$$

According to [6], the methodology of the SOM can be achieved via the processes of competition - where the Best Match Unit (BMU) is identified, cooperation -where the topological neighbourhood of the 'excited' neurons are identified and finally adaptation -where BMU and excited neurons are updated in accordance to the input vector.

In more detail the methodology of the SOM is as follows [29].

1. The weight vector of each of the neurons in the map is initialized randomly.
2. The training observed data, say x_t , is 'passed' to the map as an input vector and Euclidean distance between the all the neurons and this vector is calculated. The neuron with the smallest distance is termed the Best Matching Unit or (BMU). For each input observation, the BMU is identified. We denoted this unit as c henceforth.
3. A neighbourhood of c is selected and using a neighbourhood function given by h_{ci} , the weighted vectors of the neighbouring neurons, i are updated.

$$h_{ci}(t) = a(t) e^{-\frac{\|r_c - r_i\|^2}{2R^2(t)}} \quad (11)$$

$$W_i(t+1) = W_i(t) + h_{ci}(t) [x_t - W_i(t)] \quad (12)$$

244 Where, from equation 11, h_{ci} is the neighbouring function and t is an index of iteration, $a(t)$
245 is the learning rate, r_c is vector of c , r_i is the vector of the neuron i and R is the radius around
246 c . This function is a monotonically decreasing function of t as the learning rate decreases
247 with the iterations during the training process and the radii around c decreases with t . This
248 process ensures that neurons i closest to c are being adjusted the most.

249 The neurons are updated in accordance to equation 12 where $W_i(t+1)$ and $W_i(t)$ represent
250 the weighted vector of neuron i at the $t+1$ and t indices of iterations respectively, h_{ci} is the
251 neighbourhood function above and x_t is the observed input vector.

252 4. This process is repeated in the iterative training until the clusters are identified based on
253 their distances.

254 The data described in Section 4.2, were normalized between 0 and 1 by subtracting from each
255 element in that particular column of the data frame, its mean. These values are then divided by
256 the standard deviation of the column to give the z or standard scores. This standardizing of the
257 variables was done using the scale command. These analyses were done in R studio [30]. The
258 SOM grid was then created using the relation of 10 where $N = 52,560$ data observations for each
259 variable. The grid size used was 41 by 28 of hexagonal nodes corresponding to the factor pair of
260 1,148. This value was used instead of the calculated numeric of 1,146 because it had more factor
261 pairs.

262 The following is a list of the metrics to be plotted and their description will be shown in the
263 results section.

- 264 1. Node Count- This map gives the number of samples that are mapped to each of the nodes of
265 the map. This value should be relatively uniform throughout the SOM. Large values in some
266 areas of the map is indicative for the need of a larger map whilst empty nodes indicates that
267 a smaller map may be more appropriate. Generally, it is used to determine high density areas
268 in the map where ideally there should be a homogeneous distribution [24].
- 269 2. Neighbourhood Distance or U-Matrix- This map gives the distance between each node and its
270 neighbouring neurons. It represents the Euclidean distance amongst the codebook vectors of
271 the respective neighbourhoods [24]. Larger distances indicates dissimilarities and thus cluster
272 boundaries as nodes from the same cluster have the tendency to be closer.
- 273 3. Heat Maps - These maps separately give the distribution of each of the parameters throughout
274 the map. These are done for the four variables, both scaled and unscaled.
- 275 4. Clustering of the codebook vectors - This map consists of the codebook vectors which is the
276 data structure that carries the neuron's weight vector in a 2D grid. The number of clusters
277 or groups is input as well as the specification to add the cluster boundaries.

278 After the clusters are identified, the cluster associated with each of the $x(t)$ vectors was deter-
279 mined. Continuous intervals of the clustered 2009 Columbia, MO data set, representing approxi-
280 mately 50% and over of data points in that particular cluster, were established. There were three
281 intervals in which the majority of the vectors or rows from the data frame belonged to two of the
282 identified four clusters, denoted Cluster1 to Cluster4 (we will explain more of this in the subsequent
283 results section). For example, Interval1 ranged from 1 to 16,000 rows in which Cluster3 consisted
284 of 50.2% of the vectors. Interval2 which started at 16,001 and ended 40,500 inclusively, comprised
285 78.92% of rows from Cluster2. Interval3 included vectors from 40,501 to 52,500 in which Cluster3
286 represented approximately 48% of this interval. It should be noted that there were predominately
287 two clusters which we will also show in subsequent results of the clustering of the codebook vectors.
288 Another note to mention is that the entire time series of length was not used. Instead, 52,500 rows
289 were utilized in our analyses. There were 16,000, 24,500, and 12,000 points in Cluster1, Cluster2
290 and Cluster3 respectively.

291 These intervals are then separately trained and tested in time series forecasting using the Re-
292 current Neural Network explained in the subsequent subsection.

293 **3.3 Recurrent Neural Networks (RNN), Long Short- Term Memory Net-
294 works (LSTM)**

295 Recurrent Neural Networks (RNN) allow information to persist via one or more hidden states
296 and loops that pass information from one step to another of the network. However, for this, there
297 exists the vanishing gradient problem as the gradients asymptotically reduce to 0 from the repeated
298 multiplication of weights for various time steps. Long Short-Term Memory networks (LSTMs) are
299 a special type of RNN that can learn these long-term dependencies. The LSTM has memory blocks
300 called cells where information is stored in the cell state, c_t and the hidden state, h_t . A diagrammatic
301 representation of the architecture of such memory blocks or cells is seen in Figure 4. Information is
302 regulated by gates by optionally allowing certain data through using sigmoid and tanh activation
303 functions. The output of the sigmoid function is a number between 0 and 1, where 0 and 1 mean
304 no and all information goes to the cell state, respectively. Generally notated, the inputs to the
305 gates are the output hidden state from the previous step, h_{t-1} , and the output cell state from the
306 previous step, c_{t-1} and current input, x_t , which are pointwise multiplied by weight matrices, W ,
307 and then added to a bias, b .

308 There are three major gates: the forget, the input, and the output gates.

309 1. The forget gate: As seen in Figure 4, the input of this gate is x_t and h_{t-1} for that time
310 step. These inputs are multiplied by weight matrices and added to a bias. This value is then
311 inputted to the sigmoid function and a vector is outputted which corresponds to each value
312 in the cell state, c_{t-1} . Please refer to equation 13. This vector output is multiplied to the cell
313 state. If a 0 is output from the sigmoid function for a particular value, the forget gate wants
314 the cell state to disregard that information whilst if 1 is the sigmoid output, the forget gate
315 wants the cell state to remember this data.

$$f_t = \sigma(W_f \cdot [h_{t-1}, x_t] + b_f) \quad (13)$$

316 2. The input gate: The gate determines the information being stored in the cell state. The
317 sigmoid layer decides the data to be updated and the tanh layer, whose output values ranges
318 from -1 to 1, creates a vector of possible values that could be added to the cell state. Please
319 refer to equations 14 and 15.

$$i_t = \sigma(W_i \cdot [h_{t-1}, x_t] + b_i) \quad (14)$$

$$g_t = \tanh(W_g \cdot [h_{t-1}, x_t] + b_g) \quad (15)$$

The old cell state, c_{t-1} is then used to update the new cell state c_t . This is done representatively by equation 16. The old state is multiplied by f_t to forget the information decided upon earlier and then it is added to the product of i_t and g_t which is indicative of the new possible values scaled to the update amount decided upon for each value. Note that $*$ is representative of the Hadamard or entrywise product.

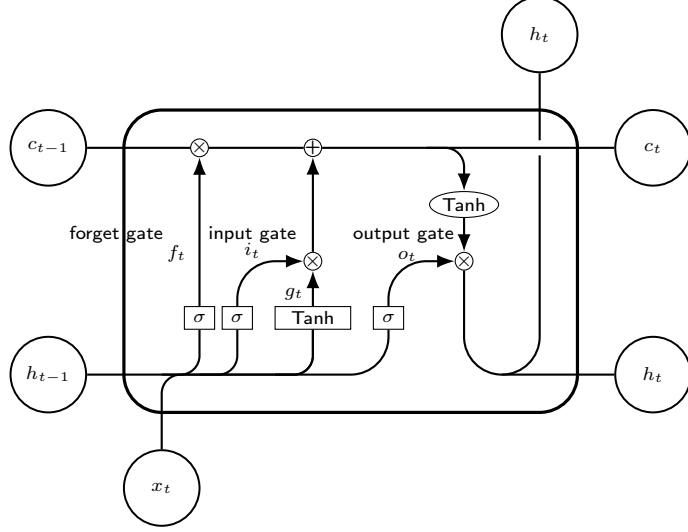
$$c_t = (f_t * c_{t-1}) + (i_t * g_t) \quad (16)$$

320 3. The output gate: A vector is created from scaling the values in the cell state using a tanh
321 function. The sigmoid function is once again used as a filter to regulate what is to be outputted
322 from the vector mentioned previously. This can be represented by equation 17. This is sent
323 as the output and as the hidden state of the next cell.

$$o_t = \sigma(W_o \cdot [h_{t-1}, x_t] + b_o) \quad (17)$$

$$h_t = o_t * \tanh(c_t) \quad (18)$$

Figure 4: LSTM Architecture



324 3.4 Moving AutoRegressive Integrated Moving Average Method (ARIMA)

325 A moving AutoRegressive Integrated Moving Average Method (ARIMA) is used as another model
 326 in our analysis. This is a statistical method which uses the relationship within the time series
 327 data in its construction. Data cannot be white noise, that is, purely random with mean = 0 and
 328 standard deviation being a constant as forecasting into the future would not be possible. If this
 329 condition is met, AutoRegressive, AR(p), Moving Average, MA(q) and AutoRegressive Moving
 330 Average, ARMA(p,q) methods can be utilized. If the data are not stationary (that is not constant
 331 mean and variances), differencing needs to be performed. An AutoRegressive Integrated Moving
 332 Average, ARIMA (p,d,q) can be used where the Integrating part represents the d or the differencing
 333 factor.

334 The AR method, a time series model, is regressed from its previous values up to an order
 335 determined by the p parameter. This can be seen mathematically from equation 19. The Partial
 336 Autocorrelation function (PACF) determines how many lags are to be incorporated in the AR
 337 method; large PACF values gives the order of the model. For lag p , the relationship between x_t
 338 and x_{t-p} is determined, filtering all the intermediate linear influence from $x_{t-1}, x_{t-2}, \dots, x_{t-(p-1)}$.

$$x_t = \beta_0 + \beta_1 x_{t-1} + \beta_2 x_{t-2} + \dots + \beta_p x_{t-p} + \varepsilon_t \quad (19)$$

339 Where x_t and x_{t-1}, \dots, x_{t-p} are the current and previous values respectively and β_0 is a constant
 340 term and β_1, \dots, β_p are the coefficient representing what part of x_{t-1}, \dots, x_{t-p} are relevant in
 341 explaining the current value etc.

342 The MA model is written in terms of a linear combination of past error. It gives the extent the
 343 series is related to its past errors. Generally it can written as equation 20. The Autocorrelation
 344 function determines the number of lags for the MA model. It is given by the lag value which is
 345 statistically different from 0 and above the error band, followed by consecutive insignificant ACF
 346 values for subsequent lags.

$$x_t = c + \varepsilon_t + \theta_1 \varepsilon_{t-1} + \theta_2 \varepsilon_{t-2} + \dots + \theta_q \varepsilon_{t-q} \quad (20)$$

347 Where x_t is the current value, ε_t and $\varepsilon_{t-1}, \dots, \varepsilon_{t-q}$ are errors from the current and previous pre-
 348 dictions respectively and $\theta_1, \dots, \theta_q$ represent the corresponding part which is relevant in explaining
 349 the current value.

350 The ARMA method is the linear combination of the linear models, AR and MA as such they too
 351 are linear models. This method thus, takes into account past values and errors in its formulation.
 352 Generally it can be written as equation 21.

$$x_t = \beta_0 + \beta_1 x_{t-1} + \beta_2 x_{t-2} + \dots + \beta_p x_{t-p} + \varepsilon_t + \theta_1 \varepsilon_{t-1} + \theta_2 \varepsilon_{t-2} + \dots + \theta_q \varepsilon_{t-q} \quad (21)$$

353 The differencing parameter, d is introduced in the ARIMA models to remove trends and seasonality.
 354 The first order difference is given by $\Delta_1 x_t = x_t - x_{t-1}$. This and higher orders can be written
 355 in terms of B , the backward shift operator where $Bx_t = x_{t-1}$ and $B(Bx_t) = B(x_{t-1}) = x_{t-2}$.
 356 Generally for shifting an observation some m periods, $B^m x_t = x_{t-m}$. Thus, the first and sec-
 357 ond differences in terms of operator B are $\Delta_1 x_t = x_t - x_{t-1} = x_t - Bx_t = (1 - B)x_t$ and
 358 $\Delta_2 x_t = \Delta_1 x_t - \Delta_1 x_{t-1} = (1 - B)^2 x_t$ respectively. The second difference can be shown to be
 359 via expansion, $x_{t-2} - 2x_{t-1} + x_t$.

360 To determine the number of differencing to use we examine the autocorrelations. If the series
 361 has positive autocorrelations out to a large number of lags then the series may need differencing.
 362 If for lag 1, the autocorrelation is zero or negative then the series does not need higher order
 363 differencing. However, if for lag 1 the autocorrelation is less than or equal to -0.5, then the series
 364 may be over-differenced. A model with no differencing implies that the series is stationary whilst the
 365 assumptions are made that for the first and second differencing of the series, the original series has a
 366 constant average trend and has time varying trends respectively. An ARIMA(1,1,0), ARIMA(0,1,1)
 367 and ARIMA(1,1,1) can be written mathematically as equations 22a and 22b, 23a and 23b, 24a and
 368 24b respectively.

$$\Delta_1 x_t = \beta_0 + \beta_1 \Delta_1 x_{t-1} \quad (22a)$$

$$\Rightarrow x_t = \beta_0 + x_{t-1} + \beta_1 (x_{t-1} - x_{t-2}) \quad (22b)$$

$$\Delta x_t = c + \Theta_1 \varepsilon_{t-1} \quad (23a)$$

$$\Rightarrow x_t = c + x_{t-1} + \Theta_1 \varepsilon_{t-1} \quad (23b)$$

$$\Delta x_t = \beta_0 + \beta_1 \Delta_1 x_{t-1} + \Theta_1 \varepsilon_{t-1} \quad (24a)$$

$$\Rightarrow x_t = \beta_0 + x_{t-1} + \beta_1 (x_{t-1} - x_{t-2}) + \Theta_1 \varepsilon_{t-1} \quad (24b)$$

369 3.5 Model Configuration

370 Model: LSTM (pressure and wind speeds as inputs) The Pytorch structure of the codes for this
 371 model was motivated/developed by [17].

- 372 • The data were loaded, preprocessed (by taking the larger wind speed of the orientations at
 373 each time step) and plotted.
- 374 • The target variable was specified as wind speed along with the forecast lead (how much we
 375 are forecasting ahead, h). The target was specified as the lag/shift of the wind speed by the
 376 forecast lead. The features were given as wind speed and pressure. The data were then split
 377 into the training (75%) and testing (25%) sets from the observations. The train and test data
 378 were then standardized where the values are not restricted to a particular bounding range
 379 like normalization.
- 380 • A sequence of observations from the train and test set were constructed. This sequence was
 381 given as a block of data from some i^{th} row - sequence length through row i . For i less than
 382 the sequence length, the 1st row was padded by repeating it as many times deemed necessary.
 383 Thus, the outputs have the number of rows in the block equal to the sequence length.
- 384 • These sequences from data set was set in Pytorch's dataloader to select minibatches. However,
 385 in our model the batch sizes selected were the entire respective train and test data sets for the
 386 Intervals. Thus we had two features (columns), fifty sequence length (rows) and one batch
 387 the length of the train and test sets.

388 • A shallow regression LSTM model was then utilized with one hidden layer of 100 hidden units.
 389 The loss function is used to calculate the error or the difference between the predicted and
 390 the actual values. The loss function chosen was Mean Square Error (MSE). The optimizer is
 391 used to make changes to the weights; it does this to try to lower the model loss function. The
 392 optimizer chosen was the Adaptive Moment Estimation (Adam) algorithm with a learning
 393 rate of 0.01. An epoch is the number of times the algorithm traverses the training data. The
 394 model was trained using 20 epochs and was then evaluated.

395 4 Results

396 From Figure 5, we can see that the elbow occurs at 4, indicative that this is the optimal k . In
 397 figure 6, 4 has the largest $S(i)$ value indicating that for $k = 4$, the objects are well matched to their
 398 respective clusters. Similarly, from Figure 7, the value which maximizes $Gap_n(k)$ is $k = 4$. From
 399 the analysis of multiple methods, the bar chart in Figure 8 indicates that most of the methods
 400 result in an optimal k of 4. This is an important consideration, as mentioned in Pearce et al. [23],
 401 because a grid with too few classes losses important information via generalizations whilst too many
 402 classes will result in loss of statistical power as there will exist smaller within class sample sizes.

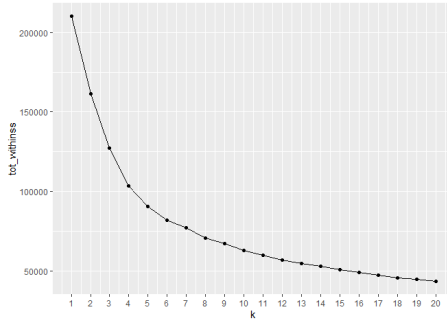


Figure 5: Elbow Method showing the optimal number of clusters of the data to be 4

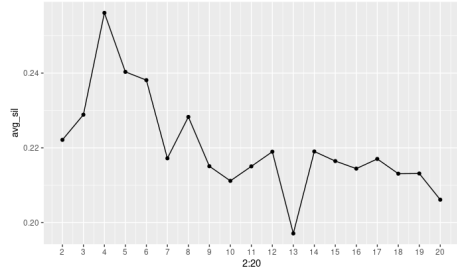


Figure 6: Silhouette Clustering Method showing the optimal number of clusters of the data to be 4

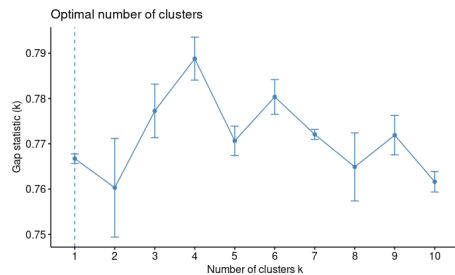


Figure 7: Gap Statistic showing the optimal number of clusters of the data to be 4

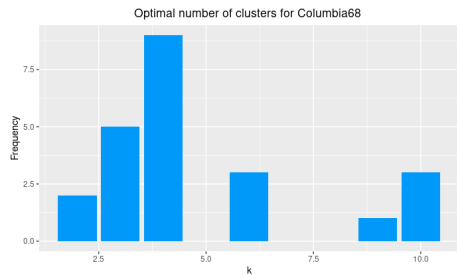


Figure 8: Methods determining optimal k show that optimally, from most methods, that $k = 4$

403 The grid was a hexagonal structure consisting of 1148 nodes. This structure consisted of no x
 404 and y axes but rather nodal positions, which were numbered as bottom left having the least value,
 405 whose node numbering increases from left to right [18]. As mentioned in [23], limitations of SOMs
 406 include its grid having a finite structure, which imposes restrictions on the map in the provision of
 407 precise information on clustering dissimilarity. Another restriction is using set of numbers to define
 408 the grid that in turn generalize its shape, be it a rectangle or a square [23].

409 From the results of the SOMs, the node count plot can be seen in Figure 9. Since the distribution
 410 of the counts is relatively uniform throughout the domain of the SOM, the map size is appropriate.
 411 Figure 10 shows the neighbourhood distance in which cluster boundaries can be identified via large
 412 nodal distances. From this map, it is evident that there exist areas where there are greater distances
 413 representative of the upper end of the scale and the lighter colours. This is seen for example in the
 414 north eastern portion of the map. From the clustering of the codebook vectors in Figure 15, we do
 415 note that this is separated as part of a cluster. This is contained in a smaller cluster whilst there
 416 are two major clusters where the adjacent nodes are grouped in the same cluster. This grid also
 417 shows, for each node, all the variables (as colour coded) in various sector representations. The radii
 418 of the sectors varies with respect to its variable [18]. The unscaled heat map for all of the variables
 419 used in this study are seen from Figures 11 to 14.

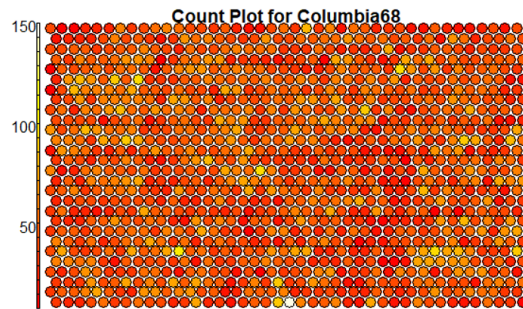


Figure 9: Node Count Plot showing the homogeneous distribution of the samples on the map

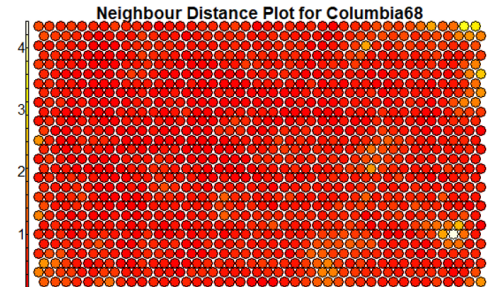


Figure 10: Neighbourhood Distance or U-Matrix showing the distance between each node and its neighbouring neurons

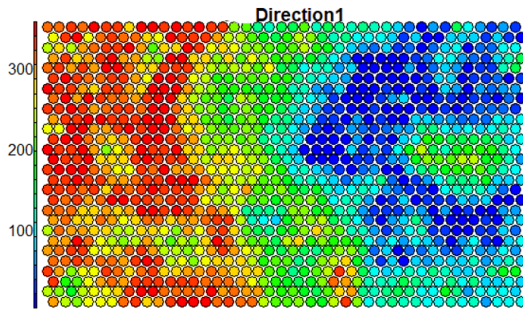


Figure 11: Heat Map showing the unscaled distribution of the wind direction values throughout the map

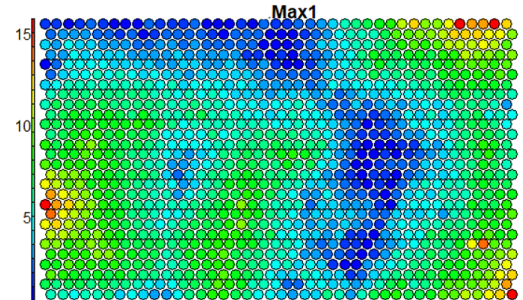


Figure 12: Heat Map showing the unscaled distribution of the wind speed values throughout the map

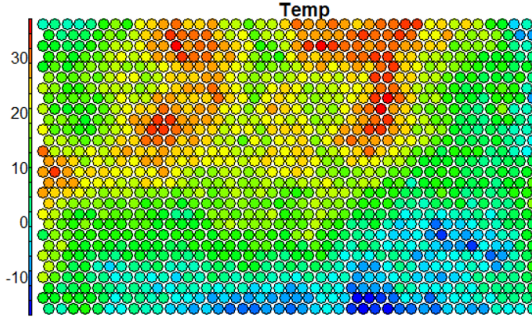


Figure 13: Heat Map showing the unscaled distribution of the temperature values throughout the map

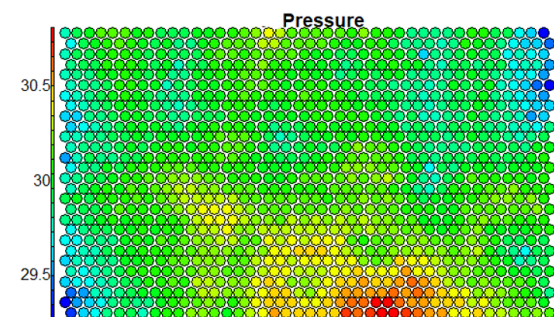


Figure 14: Heat Map showing the unscaled distribution of the pressure values throughout the map

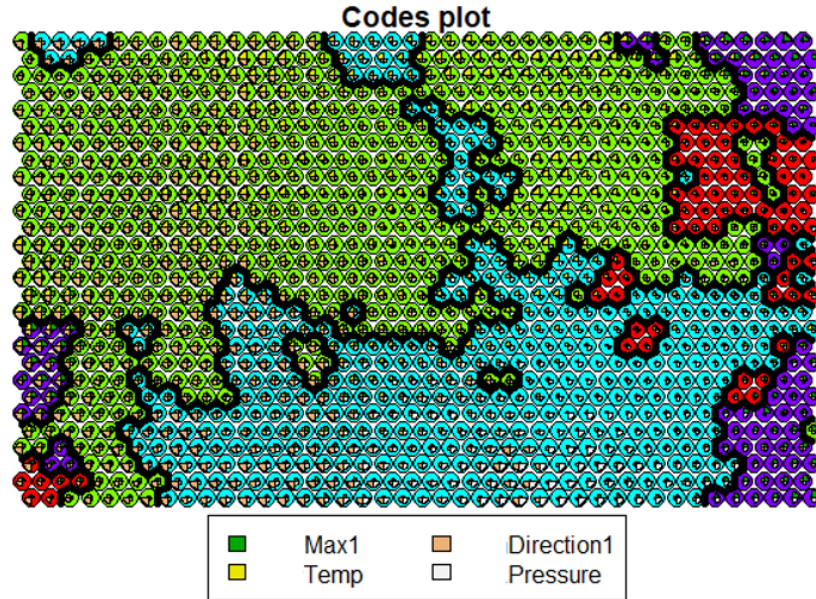


Figure 15: Clustering of codebook vectors into the optimal 4 clusters identified showing there are 2 dominant clusters

420 From the clusters of the SOMs, continuous intervals belonging to a particular cluster were
 421 identified. These intervals are representative of approximately 50% and more of the rows from the
 422 data frame belonging to a particular cluster where Interval1, Interval2 and Interval3 belonging to
 423 Cluster3, Cluster2, and Cluster3 ranged from 1 to 16,000, 16,001 to 40,500 and 40,501 to 52,500
 424 rows respectively. The three intervals identified by our clustering are graphed in Figures 16, 17 and
 425 18 where both the test and training sets are visualized. These clusters from the SOM were utilized
 426 to optimize model performance in forecasting as done in Browell et al.'s article [6]. The forecast
 427 horizon is from 20 minutes to 2 hours. As mentioned in [6], for these time scales which are used to
 428 balance the power systems by operators, statistical methodologies inclusive of ARIMA are superior
 429 to that of results obtained from Numerical Weather Predictions (NWP). This can be attributed to
 430 its low computational cost and ease of including of new data [6].

431 From table 1, the RMSE and the MAE for these intervals and various time steps, h , using the
 432 moving ARIMA model, can be seen. These values ranged from approximately 0.6 to 1.0 m s^{-1} .
 433 These results are somewhat comparable to that of [6]. Browell et al. [6] used vector autoregression
 434 in the spatial consideration of multiple locations and for this model they obtained RMSEs of 0.96 ,
 435 1.55 , 2.00 m s^{-1} for one, three and six hours ahead. Another study by [27] using both hourly and

436 10 minute data in which 39 and 173 points were forecasted respectively for each data set, have
437 RMSEs of 1.27 m s^{-1} for the hourly dataset and 0.96 m s^{-1} for the 10 minute dataset. For our
438 time step or forecast horizon of h equal to 6 (one hour ahead), for Interval1 and Interval3 this value
439 was approximately 0.8 m s^{-1} whilst for Interval2, it was an estimated 0.1 m s^{-1} less than the other
440 two intervals.

441 In our analyses, the upper and lower values from this range resulted from the run of Interval2.
442 This is expected as this interval encompassed most of the spring, all of the summer and the beginning
443 of the fall. As such it is expected that the model shows the most variability in errors for this interval.
444 It is expected as well that this interval has the lowest errors as it has highest learning ability of the
445 neurons due to its largest training set [20]. This can be seen graphically in Figure 19. From Table
446 2, we see that the results were comparable to that of the intervals defined by the SOMs. We note
447 also that spring has the largest RMSE from the moving ARIMA as expected due to the prevalence
448 of convective storms. The moving ARIMA was also trained using three quarters of the entire data
449 set, despite having this advantage of more information variability in training/learning phase, these
450 results did not deviate significantly from the interval and the seasonal analyses.

451 ANN are powerful and are frequently used in time series forecasting due to their high parallelism,
452 among other characteristics [26]. However, the ARIMA model is widely used and has given more
453 accurate results for very short term forecasts [26].

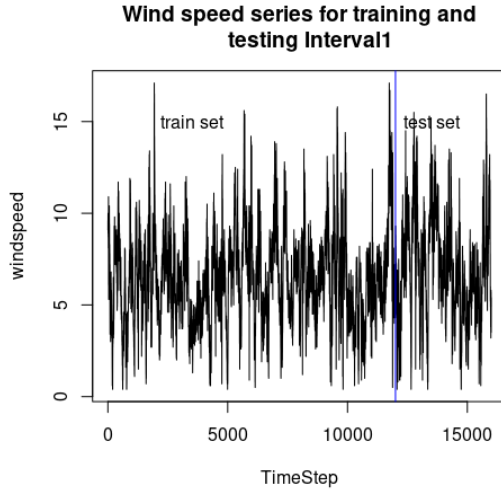


Figure 16: Interval 1 used in model runs consisting of rows 1 - 16,000 of the data

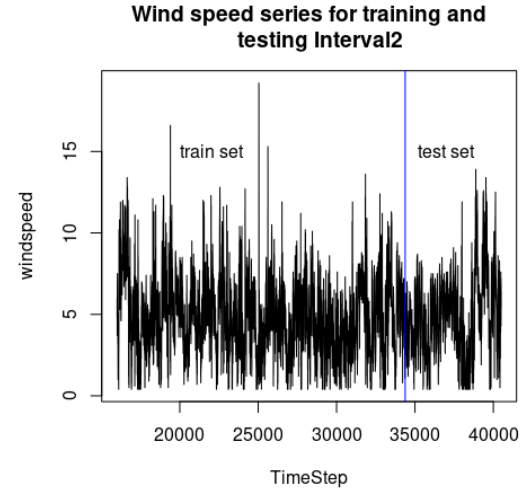


Figure 17: Interval 2 used in model runs consisting of rows 16,001 - 40,500 of the data

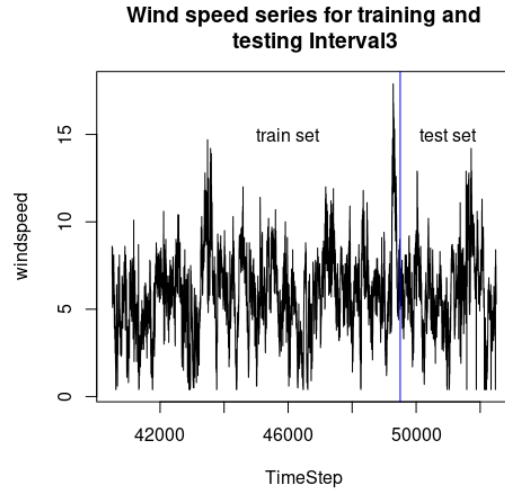


Figure 18: Interval 3 used in the model runs consisting of rows 40,501 - 52,500 of the data

Table 1: Moving ARIMA Results for the Intervals- RMSE determined for 20 to 120 minutes forecasts

h (10-mins)	Interval1 <i>RMSE</i>	Interval1 <i>MAE</i>	Interval2 <i>RMSE</i>	Interval2 <i>MAE</i>	Interval3 <i>RMSE</i>	Interval3 <i>MAE</i>
2	0.7624309	0.5587051	0.6152723	0.4480265	0.738208	0.4980114
4	0.7817789	0.5783413	0.665906	0.5017876	0.756581	0.5186229
6	0.8008848	0.5957457	0.7360105	0.5666321	0.7666935	0.5284694
8	0.8154731	0.6082994	0.8106469	0.6321702	0.7712227	0.5328341
10	0.8257323	0.6171721	0.8831231	0.6938833	0.7727915	0.5341433
12	0.832471	0.622839	0.9509406	0.7507482	0.7735839	0.5348155

Table 2: Moving ARIMA Results for 2009 data set and the seasons- RMSE determined for 20 to 120 minutes forecasts

h (10-mins)	2009 data set- RMSE	Spring- RMSE	Summer- RMSE	Fall- RMSE
2	0.6943994	0.763676	0.5139139	0.6625789
4	0.711852	0.7787825	0.5504232	0.68182
6	0.730347	0.7998983	0.5724217	0.7019841
8	0.7445687	0.8185765	0.5821634	0.7278857
10	0.7543516	0.8330311	0.5854124	0.7558021
12	0.7608936	0.8438839	0.5858682	0.7844518

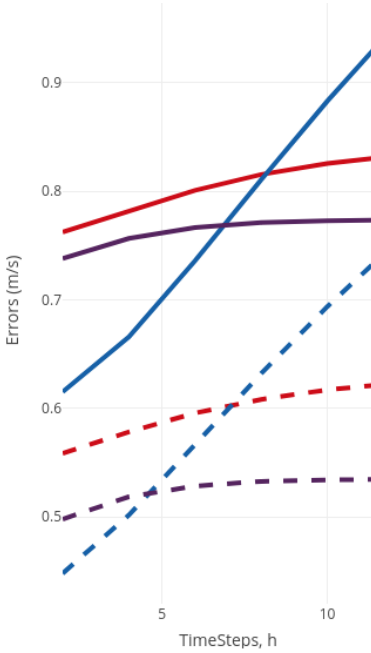


Figure 19: ARIMA Errors for the Intervals- RMSE for 20 to 120 minutes forecasts shows that Interval2 which consists of most of spring, all of summer and the beginning of fall, has the largest range of errors

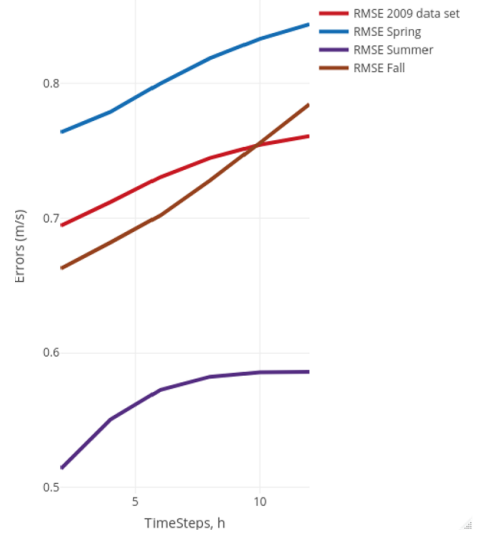


Figure 20: ARIMA Errors for 2009 data set and the seasons- RMSE for 20 to 120 minutes forecasts shows that summer and spring have the least and most errors respectively

454 The LSTM methodology was applied for the wind speed and pressure time series. Pressure was
 455 chosen because it had the greatest magnitude correlation with wind speed when compared with the
 456 other meteorological variables of wind direction and temperature. The RMSE results can be seen
 457 from Table 3. The test forecasted series for the various intervals, together with the actual series,
 458 can be seen in Figures 21 to 23. From the results obtained, ARIMA incurs smaller RMSE than
 459 the LSTM model for all intervals. Though there have been studies for which ARIMA outperforms
 460 ANN and SVM as mentioned in [27], there have been RNN methods used in wind speed forecasting
 461 which performs better than ARIMA. In [27], the errors are approximately 11 to 14 percent less in
 462 the RNN model compared to their ARIMA method. Another study, [9], univariate ARIMA saw
 463 higher errors than univariate RNN. The same result was observed when comparing multivariate
 464 ARIMA with a multivariate RNN.

465 The reason for such results can be attributed to the difficulty of representing the high dimen-
 466 sional and non-linear system using the one-dimensional wind speed time series [15]. As such the
 467 series is lagged using the time delay τ and the embedding dimension d for each of the intervals and
 468 these lagged co-ordinates were input to the LSTM model. The τ value was determined to be 3

469 using Auto Mutual Information (AMI) with the exception of Interval2 whose value was given by 2.
 470 The d value was determined to be 6 using Cao Algorithm for all intervals. The τ value was taken
 471 at the first local minimum for the AMI and the d value, as when $E1(d)$ attains saturation. Please
 472 refer to [3] for more information on the methodologies of these parameters as well as Figures 24
 473 and 25. Another study that uses the lags of the series in the training of the ANN as input variables
 474 was [8]. It was determined in their study that the best model was the simplest consisting of two
 475 layers and two input and one output neurons [8].

476 The results obtained can be seen in Figures 26 to 28 for Interval1 to Interval3 respectively. The
 477 persistence model for each interval was constructed by calculating the average for every multiple
 478 of the 6th hour and recording these as the values of persistence for the next consecutive 6 hours
 479 or 36 time steps. The time forecast horizon, h looked at for this analysis are 60, 120, 180, 240,
 480 300 and 360 minutes. The models under comparison are the LSTM with lagged wind speeds as
 481 inputs, the Moving ARIMA, the LSTM with pressure and wind speeds as inputs and persistence.
 482 The Normalized Root Mean Squared Error (NRMSE) metric for model evaluation was determined
 483 for all of the models. For values of this metric exceeding 1 or 100% implies that the forecast is no
 484 better than the mean of the data after this run.

485 It can be noted that all models performed better than the persistence model which stayed con-
 486 sistently between 0.8 and approximately 1.0 for the three intervals. The h value of 360 minutes for
 487 Interval1 and Interval2 have values which are over 1.0 or representative of a forecast no better than
 488 the mean. The LSTM with the lagged wind speeds as inputs, denoted as Lagseries, outperformed
 489 the LSTM with the pressure and wind speeds as inputs, denoted as Pressureandwind, for all of the
 490 intervals. The Moving ARIMA method is now beaten by the lagged LSTMs for up to the 180th
 491 minute time step in Interval2 and up to the 120th time forecast horizon in Interval1 and Interval3.
 492 The second interval as mentioned previously has most of spring which have convective storm
 493 events, so it is expected that if any interval is to do best in the non-linear model of the LSTM when
 494 compared to the linear model of the ARIMA model, it would have been Interval2. The NRMSE
 495 of the LSTM Pressureandwind tends to one faster than the LSTM Lagseries for all of the intervals
 496 though up to the h value of 360 minutes, they do not exceed 1. As expected when the entire test
 497 set was forecasted for the models ($h =$ test set), the NRMSE for most of the intervals exceeded 1;
 498 for the other cases, they were 0.97 and 0.98.

499 The tabulated results of the RMSE values for each of these models can be seen in Table 4. The
 500 forecasted and the actual series for $h = 360$ minutes for LagSeries1 to LagSeries3 can be seen in
 501 Figures 29 to 31 respectively. Similarly, these plots for the ARIMA1 to ARIMA3 test set can be
 502 seen in subsequent figures whilst correspondingly the error defined as the difference between the
 503 actual test data and the predicted test data can be viewed in Figures 35 to 37. It can be noted,
 504 especially for the Moving ARIMA results, there was a significant match between the predicted and
 505 the actual series. The differences in the actual test data and the predicted test data were varying
 506 about the zero marker thus indicating that the trends were well captured by the model.

Table 3: LSTM (with pressure and wind as inputs) RMSE values indicate that the Moving ARIMA beats the LSTM for forecast times of 20 to 120 minutes

h (10-mins)	Interval1- RMSE	Interval2- RMSE	Interval3- RMSE
2	0.940142796	0.975498677	0.834158971
4	1.155461471	1.219467954	0.927660403
6	1.296958276	1.257914418	0.992396502
8	1.444971761	1.35340903	1.026433109
10	1.451004208	1.432323828	1.137951695
12	2.767638696	1.502783097	1.14651633

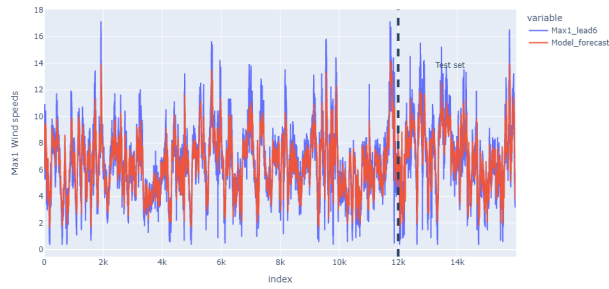


Figure 21: LSTM Interval1 showing the model forecast of forecast time 60 minutes or 1 hour and the actual wind speed values, $Max1$

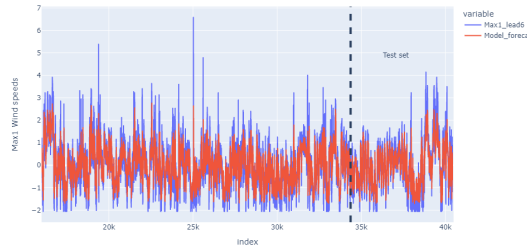


Figure 22: LSTM Interval2 showing the model forecast of forecast time 60 minutes or 1 hour and the actual wind speed values, $Max1$

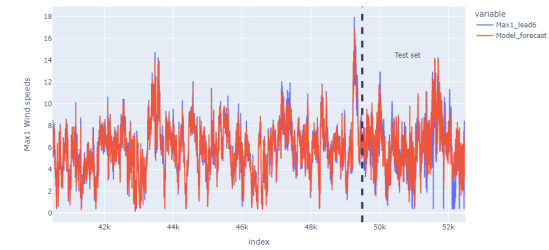


Figure 23: LSTM Interval3 showing the model forecast of forecast time 60 minutes or 1 hour and the actual wind speed values, $Max1$

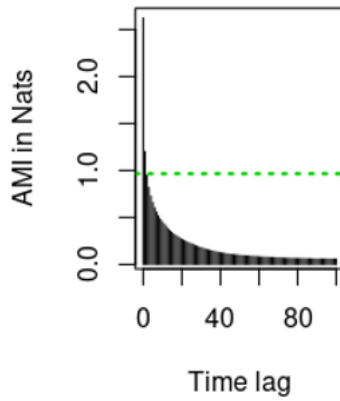


Figure 24: Tau or time delay for Interval2 is given by 2 using the Auto Mutual Information (AMI)

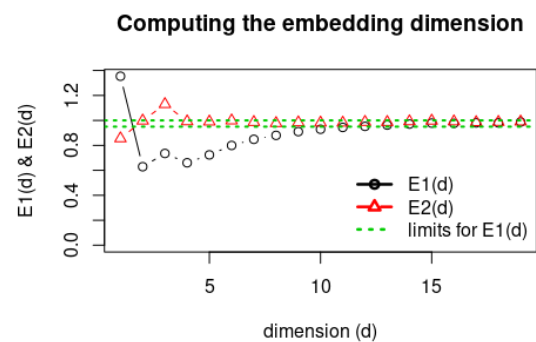


Figure 25: Embedding dimension for Interval2 is determined to be 6 from Cao Algorithm

NRMSE for Interval1

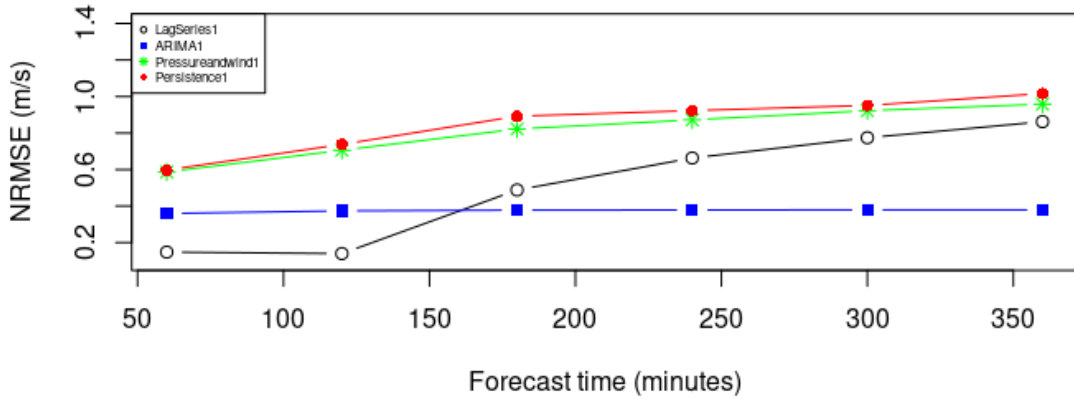


Figure 26: NRMSE for Interval1 using Models- LagSeries1 which is the LSTM with lagged wind speeds as inputs, ARIMA1 which is the Moving ARIMA model, Pressureandwind1 which is the LSTM with pressure and wind speeds as inputs and Persistence1 which is the Persistence model. The LagSeries1 improves upon Pressureandwind1 and beats the Moving ARIMA for forecast times of 60 and 120 minutes

NRMSE for Interval2

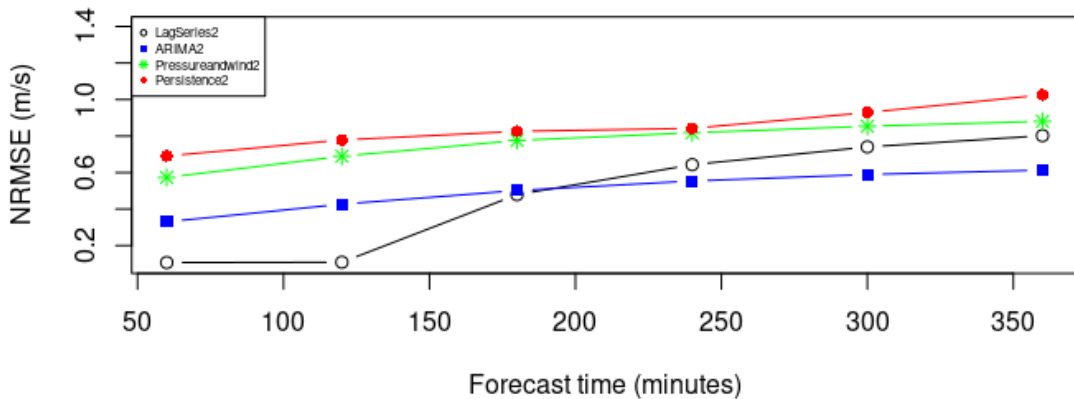


Figure 27: NRMSE for Interval2 using Models- LagSeries2 which is the LSTM with lagged wind speeds as inputs, ARIMA2 which is the Moving ARIMA model, Pressureandwind2 which is the LSTM with pressure and wind speeds as inputs and Persistence2 which is the Persistence model. The LagSeries2 improves upon Pressureandwind2 and beats the Moving ARIMA for forecast times of 60, 120 and 180 minutes

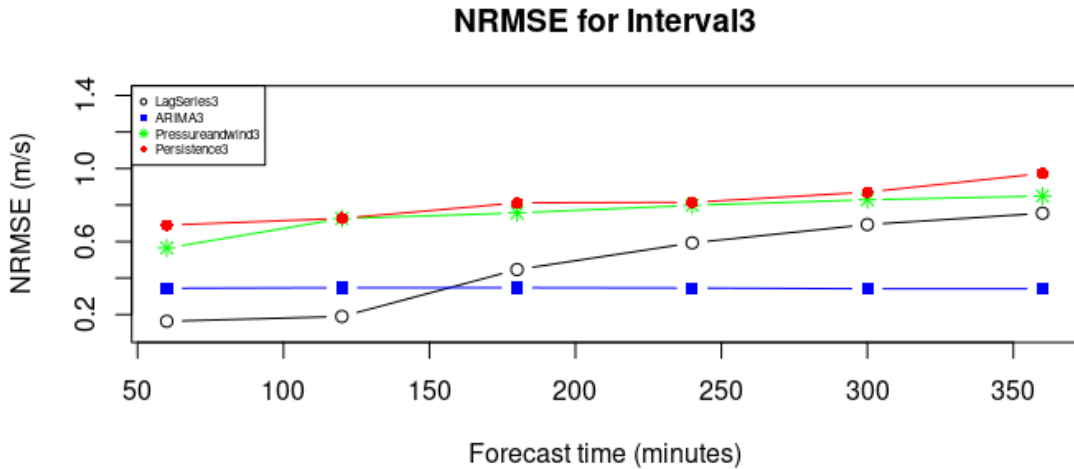


Figure 28: NRMSE for Interval3 using Models- LagSeries3 which is the LSTM with lagged wind speeds as inputs, ARIMA3 which is the Moving ARIMA model, Pressureandwind3 which is the LSTM with pressure and wind speeds as inputs and Persistence3 which is the Persistence model. The LagSeries3 improves upon Pressureandwind3 and beats the Moving ARIMA for forecast times of 60 and 120 minutes

Table 4: Models' RMSE Results for the Intervals showing that the best performing model, up to 180 minutes or 3 hours, is LagSeries

Interval	h (mins)	LagSeries	ARIMA	Pressureandwind	Persistence
Interval1	60	0.372907494	0.8008848	1.307214932	1.331339773
	120	0.352250278	0.832471	1.572144369	1.643609466
	180	1.087379921	0.8412903	1.831567231	1.987401039
	240	1.477212704	0.8436806	1.943241466	2.055514112
	300	1.724707138	0.8443778	2.05444378	2.119308164
	360	1.920543992	0.8444589	2.13412727	2.263135526
Interval2	60	0.238592146	0.7360105	1.276806808	1.538227218
	120	0.242534049	0.9509406	1.53582464	1.734079072
	180	1.067046011	1.117465	1.72837262	1.83946146
	240	1.432849673	1.233804	1.822299134	1.875548504
	300	1.649253577	1.312496	1.9014607	2.069048477
	360	1.786658699	1.365862	1.961462493	2.284102311
Interval3	60	0.376359712	0.7666935	1.257796263	1.536880065
	120	0.436734176	0.7735839	1.617069345	1.619311738
	180	1.028754688	0.7734066	1.685952464	1.80858766
	240	1.36522671	0.7698904	1.778578867	1.814853169
	300	1.596357379	0.7602228	1.84599341	1.939363159
	360	1.739204251	0.7602228	1.891493873	2.168188039

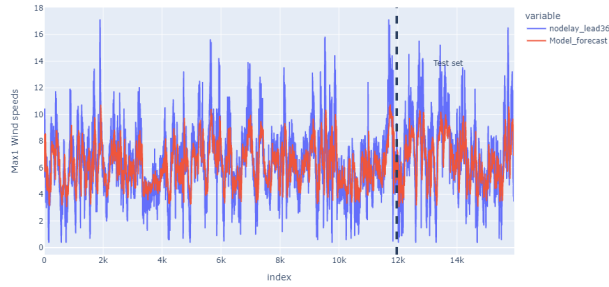


Figure 29: LagSeries1 LSTM showing the model forecast of prediction time, 6 hours and the actual wind speed values, *Max1*

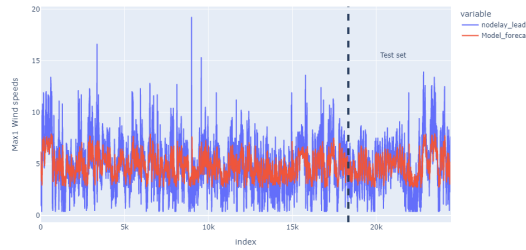


Figure 30: Lagseries2 LSTM showing the model forecast of prediction time, 6 hours and the actual wind speed values, *Max1*

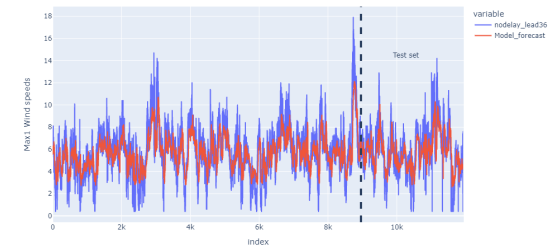


Figure 31: LagSeries3 LSTM showing the model forecast of prediction time, 6 hours and the actual wind speed values, *Max1*

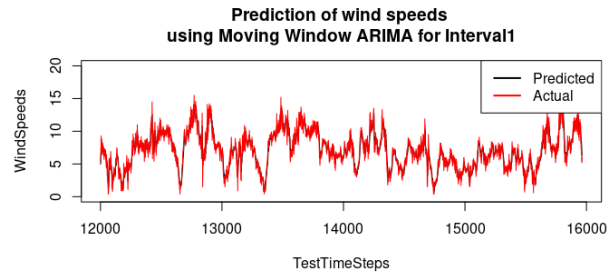


Figure 32: Predictions of Moving ARIMA1 for forecast time, 6 hours and the actual wind speed values

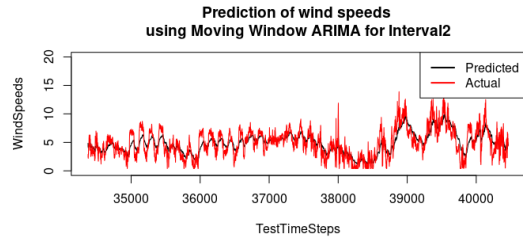


Figure 33: Predictions of Moving ARIMA2 for forecast time, 6 hours and the actual wind speed values

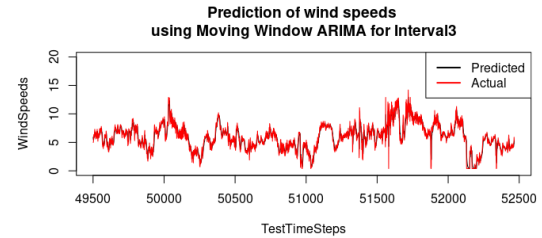


Figure 34: Predictions of Moving ARIMA3 for forecast time, 6 hours and the actual wind speed values

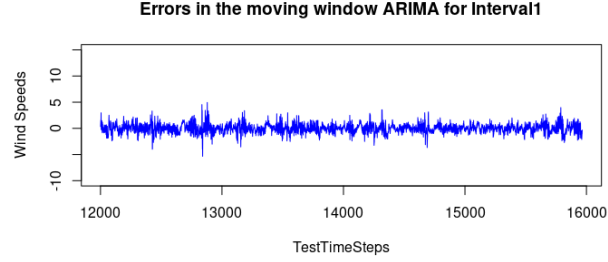


Figure 35: Errors of Moving ARIMA1 for forecasting time, 6 hours, of the test time series

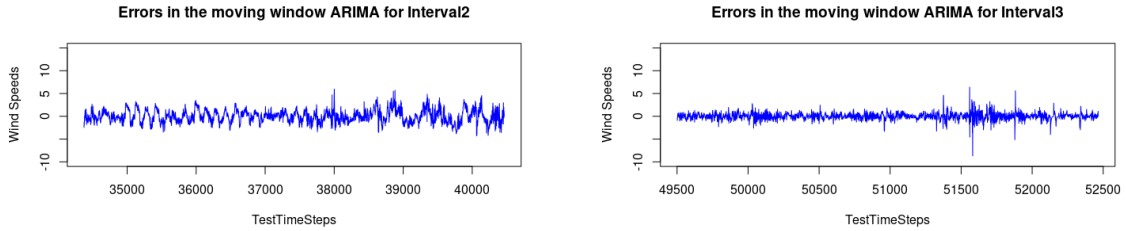


Figure 36: Errors of Moving ARIMA2 for forecasting time, 6 hours, of the test time series

Figure 37: Errors for Moving ARIMA3 for forecasting time, 6 hours, of the test time series

507 5 Future Work, Additional Analyses and Conclusion

508 In the model runs, the forecast variable - in our case wind speed - can be further processed to
 509 determine if there are any patterns in the wind speed forecast values (in terms of its accuracy) when
 510 its actual values is less than or greater than some x value or the difference between consecutive
 511 actual values rates are higher than some y value.

512 Yearly analysis can be done to see if there are the same number of clusters and accuracy in
 513 forecasting (seasonal analysis - using yearly data) is similar.

514 The optimal number of clusters was determined to be 4 using the Elbow and Silhouette methods
 515 among others. SOMs were then used to cluster the data after which three continuous intervals
 516 belonging to a particular cluster, which represented approximately 50% and over of the input
 517 vectors or rows from the data frame were identified. These intervals were then inputs for the
 518 LSTMs with inputs pressure and wind speeds, the lagged series LSTMs with embedding dimension
 519 d and time delay τ , the Moving Window ARIMA and persistence models. It was determined that
 520 the Moving ARIMA model is outperformed by the lagged LSTM for at most 180 minutes from the
 521 runs of the defined intervals. The lagged series improved upon the LSTM with the wind speed and
 522 pressure series. All of these models however, performed better than the benchmark of persistence
 523 for all time steps.

524 References

- 525 [1] V. Bali, A. Kumar, and S. Gangwar. A novel approach for wind speed forecasting using
 526 lstm-arima deep learning models. International Journal of Agricultural and Environmental
 527 Information Systems (IJAEIS), 11(3):13–30, 2020.
- 528 [2] S. Balkissoon, N. Fox, and A. Lupo. Fractal characteristics of tall tower wind speeds in
 529 missouri. Renewable Energy, 154:1346–1356, 2020.
- 530 [3] S. Balkissoon, N. Fox, A. Lupo, S. E. Haupt, Y. C. Li, P. Market, and S. Walsh. Determining
 531 chaotic characteristics and forecasting tall tower wind speeds in missouri using empirical
 532 dynamical modeling (edm). Renewable Energy, 170:1292–1307, 2021.

533 [4] I. A. Basheer and M. Hajmeer. Artificial neural networks: fundamentals, computing, design,
 534 and application. *Journal of microbiological methods*, 43(1):3–31, 2000.

535 [5] S. Berkovic. Winter wind regimes over israel using self-organizing maps. *Journal of Applied
 536 Meteorology and Climatology*, 56(10):2671–2691, 2017.

537 [6] J. Browell, D. R. Drew, and K. Philippopoulos. Improved very short-term spatio-temporal
 538 wind forecasting using atmospheric regimes. *Wind Energy*, 21(11):968–979, 2018.

539 [7] J. C. Burguillo. Using self-organizing maps with complex network topologies and coalitions
 540 for time series prediction. *Soft Computing*, 18(4):695–705, 2014.

541 [8] E. Cadenas and W. Rivera. Short term wind speed forecasting in la venta, oaxaca, méxico,
 542 using artificial neural networks. *Renewable Energy*, 34(1):274–278, 2009.

543 [9] Q. Cao, B. T. Ewing, and M. A. Thompson. Forecasting wind speed with recurrent neural
 544 networks. *European Journal of Operational Research*, 221(1):148–154, 2012.

545 [10] M. Elsaraiti and A. Merabet. A comparative analysis of the arima and lstm predictive models
 546 and their effectiveness for predicting wind speed. *Energies*, 14(20):6782, 2021.

547 [11] N. I. Fox. A tall tower study of missouri winds. *Renewable Energy*, 36(1):330–337, 2011.

548 [12] R. Fukuoka, H. Suzuki, T. Kitajima, A. Kuwahara, and T. Yasuno. Wind speed prediction
 549 model using lstm and 1d-cnn. *Journal of Signal Processing*, 22(4):207–210, 2018.

550 [13] S. Gangwar, V. Bali, and A. Kumar. Comparative analysis of wind speed forecasting using
 551 lstm and svm. *EAI Endorsed Transactions on Scalable Information Systems*, 7(25):e1–e1, 2020.

552 [14] D. Geng, H. Zhang, and H. Wu. Short-term wind speed prediction based on principal com-
 553 ponent analysis and lstm. *Applied Sciences*, 10(13):4416, 2020.

554 [15] R. Hu, W. Hu, N. Gökmen, P. Li, Q. Huang, and Z. Chen. High resolution wind speed
 555 forecasting based on wavelet decomposed phase space reconstruction and self-organizing map.
 556 *Renewable Energy*, 140:17–31, 2019.

557 [16] H. Kalinić, F. Matić, H. Mihanović, I. Vilibić, N. Žagar, B. Jasenko, and M. Tudor. Comparison
 558 of two meteorological models using self-organizing maps. In *OCEANS 2015-Genova*, pages 1–6.
 559 IEEE, 2015.

560 [17] B. Kent. How to use pytorch lstms for time series regression.
 561 <https://www.crosstab.io/articles/time-series-pytorch-lstm>.

562 [18] S. Lakshminarayanan. Application of self-organizing maps on time series data for identifying
 563 interpretable driving manoeuvres. *European transport research review*, 12(1):1–11, 2020.

564 [19] G. Li and J. Shi. On comparing three artificial neural networks for wind speed forecasting.
 565 *Applied Energy*, 87(7):2313–2320, 2010.

566 [20] G.-F. Lin, T.-C. Wang, and L.-H. Chen. A forecasting approach combining self-organizing
 567 map with support vector regression for reservoir inflow during typhoon periods. *Advances in
 568 Meteorology*, 2016, 2016.

569 [21] M. C. Mabel and E. Fernandez. Analysis of wind power generation and prediction using ann:
 570 A case study. *Renewable energy*, 33(5):986–992, 2008.

571 [22] V. Nourani, A. H. Baghanam, V. Vousoughi, and M. Alami. Classification of groundwater level
 572 data using som to develop ann-based forecasting model. *Int J Soft Comput Eng*, 2(1):2231–07,
 573 2012.

574 [23] J. L. Pearce, L. A. Waller, H. H. Chang, M. Klein, J. A. Mulholland, J. A. Sarnat, S. E. Sarnat,
 575 M. J. Strickland, and P. E. Tolbert. Using self-organizing maps to develop ambient air quality
 576 classifications: a time series example. *Environmental Health*, 13(1):1–14, 2014.

577 [24] R. Rakotomalala. Tanagra data mining. Version, 1:39, 2005.

578 [25] P. Ramasamy, S. Chandel, and A. K. Yadav. Wind speed prediction in the mountainous region
579 of india using an artificial neural network model. Renewable Energy, 80:338–347, 2015.

580 [26] N. Ramesh Babu and P. ArulmozhiVarman. Forecasting of wind speed using artificial neural
581 networks. Int. Rev. Mod. Sim., 5(5), 2012.

582 [27] K. Sandhu, A. R. Nair, et al. A comparative study of arima and rnn for short term wind
583 speed forecasting. In 2019 10th International Conference on Computing, Communication and
584 Networking Technologies (ICCCNT), pages 1–7. IEEE, 2019.

585 [28] A. Sfetsos. A comparison of various forecasting techniques applied to mean hourly wind speed
586 time series. Renewable energy, 21(1):23–35, 2000.

587 [29] J. Tian, M. H. Azarian, and M. Pecht. Anomaly detection using self-organizing maps-based
588 k-nearest neighbor algorithm. In PHM Society European Conference, volume 2, 2014.

589 [30] R. Wehrens, L. M. Buydens, et al. Self-and super-organizing maps in r: the kohonen package.
590 Journal of Statistical Software, 21(5):1–19, 2007.

591 [31] Y.-X. Wu, Q.-B. Wu, and J.-Q. Zhu. Data-driven wind speed forecasting using deep feature
592 extraction and lstm. IET Renewable Power Generation, 13(12):2062–2069, 2019.

593 [32] M. Yan and K. Ye. Determining the number of clusters using the weighted gap statistic.
594 Biometrics, 63(4):1031–1037, 2007.

595 [33] W. Yao, P. Huang, and Z. Jia. Multidimensional lstm networks to predict wind speed. In 2018
596 37th Chinese Control Conference (CCC), pages 7493–7497. IEEE, 2018.

597 [34] U. Zaman, H. Teimourzadeh, E. H. Sangani, X. Liang, and C. Y. Chung. Wind speed fore-
598 casting using arma and neural network models. In 2021 IEEE Electrical Power and Energy
599 Conference (EPEC), pages 243–248. IEEE, 2021.